Water Resources Research

RESEARCH ARTICLE
10.1029/2019WR025131

Mean Velocity and Shear Stress Distribution in Floating Treatment Wetlands: An Analytical Study

Shuolin Li[1,2], **Gabriel Katul**[2,3], **and Wenxin Huai**[4]

[1]Sibley School of Mechanical and Aerospace Engineering, Cornell University, Ithaca, NY, USA, [2]Nicholas School of the Environment, Duke University, Durham, NC, USA, [3]Department of Civil and Environmental Engineering, Duke University, NC, Durham, USA, [4]State Key Laboratory of Water Resources and Hydropower Engineering Science, Wuhan University, Wuhan, China

Key Points:
- A two-domain analytical model for flow inside floating treatment wetlands (FTWs) is proposed
- The model accounts for the shear stress asymmetry bounding the vegetation-free zone below the FTW
- The model recovers the mean velocity and shear stress profiles reported in laboratory experiments configured to resemble FTW

Correspondence to:
W. Huai,
wxhuai@whu.edu.cn

Citation:
Li, S., Katul, G., & Huai, W. (2019). Mean velocity and shear stress distribution in floating treatment wetlands: An analytical study. *Water Resources Research*, *55*. https://doi.org/10.1029/2019WR025131

Received 10 MAR 2019
Accepted 11 JUL 2019
Accepted article online 16 JUL 2019

Abstract Floating treatment wetlands (FTWs) are efficient at wastewater treatment; however, data and physical models describing water flow through them remain limited. A two-domain model is proposed dividing the flow region into an upper part characterizing the flow through suspended vegetation and an inner part describing the vegetation-free zone. The suspended vegetation domain is represented as a porous medium characterized by constant permeability thereby allowing Biot's Law to be used to describe the mean velocity and stress profiles. The flow in the inner part is bounded by asymmetric stresses arising from interactions with the suspended vegetated (porous) base and solid channel bed. An asymmetric eddy viscosity model is employed to derive an integral expression for the shear stress and the mean velocity profiles in this inner layer. The solution features an asymmetric shear stress index that reflects two different roughness conditions over the vegetation-induced auxiliary bed and the physical channel bed. A phenomenological model is then presented to explain this index. An expression for the penetration depth into the porous medium defined by 10% of the maximum shear stress is also derived. The predicted shear stress profile, local mean velocity profile, and bulk velocity agree with the limited experiments published in the literature.

1. Introduction

Ponds and wetlands have been used as low-cost and low-maintenance stormwater treatment facilities while offering esthetic and recreational benefits (de Stefani et al., 2011; Khan et al., 2013; Leiva et al., 2018; Sun et al., 2009). However, traditional surface flow wetlands with aquatic vegetation growing in sediments are susceptible to damage because of excessive inundation and rapid transients in water level. Floating treatment wetlands (FTWs) may provide an alternative, especially for stormwater treatment. FTWs are artificial platforms (or mats) that permit aquatic emergent vegetation to grow in water that may be otherwise too deep for them. Their roots develop through a floating platform into the water creating a matrix characterized by a large surface area to volume ratio. This dense matrix traps nutrients and contaminants that then support microbes responsible for the creation of a biofilm where much of the biodegradation occurs. The microbes living within the matrix convert nitrite-nitrogen (NO_2-N) to nitrogen gas (NH_3-N) through nitrate reduction (Randall et al., 1998; Wells et al., 2017). In addition, plants directly absorb nutrients from the water column instead of sediments, which then increases the overall absorption efficiency (Headley et al., 2008). As a result, overall uptake rates of contaminants and nutrients are increased over conventional wetlands.

The description of the transport and contaminant removal mechanisms within FTWs are still far from complete. For example, de Stefani et al. (2011) conducted a series of experiments in natural rives and reported that the chemical oxygen demand decreased by up to 66% once the FTW covers were implemented. As they state, such a large chemical oxygen demand sink requires inquiry into both—the physical processes and chemical/biological transformations occurring in the FTW. Any assessment of contaminant and nutrient removal by FTWs must begin by describing the simultaneous water transport within and below the mat-root system. The absence of such a model hinders the utility of FTWs as viable engineering phytoremediation options. To be clear, developing such a model is by no means sufficient to tackle all the complex biological and chemical transformation issues occurring in FTW though it may be deemed as a necessary and logical first step. The study here seeks to begin addressing this knowledge gap by developing a reduced but physically based model describing the mean velocity and turbulent stress profiles within an idealized FTW. The

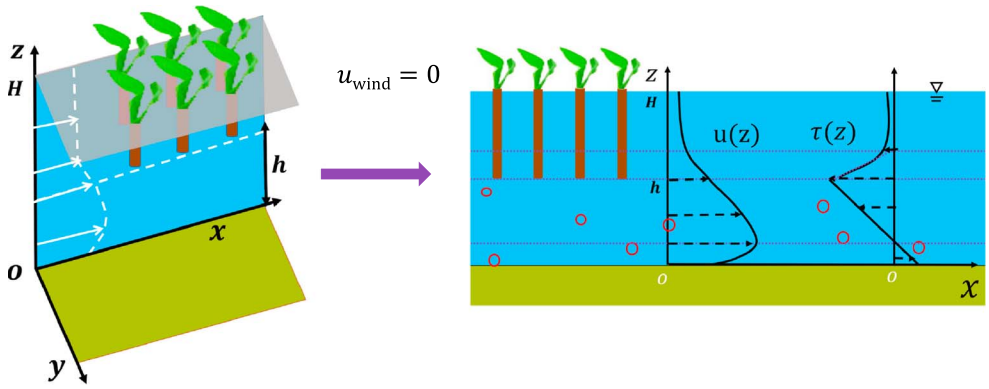

Figure 1. (left) The two-domain system used to approximate the flow through a simplified FTW, where H is the flow depth and h is the thickness of the flow region beneath the suspended canopy. Surface winds are momentarily ignored in this initial consideration. (right) The expected shapes of the mean velocity $u(z)$ and shear stress $\tau(z)$ profiles are shown, where x and z represent the streamwise and vertical directions, respectively. The intermediate layer is part of the suspended canopy domain characterized by a rapid decline in $\tau(z)$ with increasing z.

starting point is the suspended canopy model originally proposed by Plew (2010) whose components are sketched in Figure 1. The suspended canopy is represented by densely packed smooth rigid rods mirroring the root-porous system anchored to the top of the water surface.

Figure 1 suggests that the flow domain within a canonical FTW system is characterized by two regions and three layers. The two regions are the dense rigid but floating vegetation and the vegetation-free region below it. The three layers are as follows: An upper layer where the mean velocity profile is roughly uniform and the shear stress is small. In this layer, the flow is analogous to those encountered in porous media where nonlinear or inertial correction to Darcy's law (i.e., Forchheimer effects) may be included. A bottom vegetation-free layer that resembles a channel flow where the channel bottom experiences conventional wall friction but the top experiences finite shear stresses, mean velocity, and mean velocity gradients. An "intermediate" layer must then form at the bottom of the floating vegetation layer where the flow transitions from channel-like (often turbulent state) to a porous-medium-like. A mathematical model describing the entire mean velocity and shear stress profiles are to be developed based on the expected physics in this three-layer representation here. Comparisons with published experiments collected separately for various layers suggest that the proposed model and representations can reasonably reproduce the essential features of the mean velocity and shear stress profile shapes in FTWs.

2. Theory

Throughout, the coordinate system is as follows: x represents the longitudinal direction, y represents the lateral direction, and z represents the vertical direction with $z = 0$ being the channel bottom. The flow in the FTW featured in Figure 1 is assumed to be steady and uniform so that the flow depth H is constant. The FTW is assumed to be sufficiently wide so that any side friction can be ignored relative to other frictional forces resisting water movement in both domains. The FTW is also assumed to be sloped with a small sloping angle θ so that $\tan(\theta) = \sin(\theta)$.

The suspended canopy is composed of uniform rigid cylinders of height h placed at high density defined by the number of cylinders per unit ground area. The suspended canopy region is further divided into two dynamically distinct layers. An upper layer that is to be modeled as a porous medium and a lower layer impacted by the flow in the vegetation-free domain. Hereafter, this vegetation-free layer is simply referred to as the inner layer. The flow velocity in the canopy layer is expected to be relatively large so that turbulent shear stresses cannot be entirely ignored. With some modifications, a porous-media assumption for the upper canopy layer is to be employed based on its success in several obstructed open flow systems including submerged canopy flows (Battiato & Rubol, 2014; Rubol et al., 2016, 2018; Wang & Huai, 2018.)

Airflow above the FTW in Figure 1 is momentarily ignored so that any air-induced stresses at the air-water interface is assumed to be negligible or absorbed by the aerial part of the suspended canopy. Moreover, water density gradients within the FTW are ignored as well.

Flow in the inner layer ($z \in [h, H]$) is complicated by the fact that the top and bottom are experiencing different types of frictional resistance. One type is associated with the frictional stress generated by the canopy (or porous medium) bottom and the other type is a conventional frictional stress generated by the channel bed that can be either smooth, rough, or transitional. For this reason, a dimensionless stress index λ is introduced and defined as $\lambda^2 = \tau_v/\tau_b$ or as $\lambda = u_{*v}/u_{*b}$. This stress index is used to assess the degree of stress asymmetry experienced by the inner layer and its inference is to be explored later on. Here, τ_v and u_{*v} are the shear stress and associated friction velocity at the bottom of the canopy layer, and τ_b and u_{*b} are the shear stress and friction velocity at the channel bed, respectively. Physically, λ reflects the effects of the vegetation roughness and river bed roughness on the flow in the inner layer. For example, if $\lambda \gg 1$, the canopy roughness is more significant than the channel roughness.

The novelties of the proposed model are in the treatment of the inner layer, its coupling to the floating vegetation layer, and the representation of the properties of the floating vegetation layer. The inner layer is considered integrally thereby avoiding the need to explicitly resolve all its subdomains as previously proposed in similar asymmetric shear flows (Huai et al., 2012). The vegetation layer is further characterized by an obstruction permeability as suggested elsewhere (Battiato & Rubol, 2014; Lowe et al., 2008), which differs from prior cylindrical drag force representation involving unknown drag coefficients or patterns and bending status of cylinders. This approximate treatment of the flow within the vegetation layer (Battiato & Rubol, 2014; Rubol et al., 2016) allows the use of Biot's Law (Biot, 1956; Hu et al., 2014; Zhao et al., 2012) to describe the mean velocity. In Biot's derivation, tortuosity characterizes the heterogeneity of the local velocity that can then be simplified and expressed as a function of the mean local velocity. Furthermore, a vertical momentum dispersivity component can be linearly introduced and used to capture the stem-scale turbulence as discussed elsewhere (Zeng & Chen, 2011).

2.1. Governing Equations

The continuity and momentum equations governing the flow in a porous medium (Biot's Law) are given as

$$\frac{\partial}{\partial t}(n\rho) + \bigtriangledown \cdot (n\rho \mathbf{U}) = 0; \quad n\rho \frac{D\mathbf{U}}{Dt} = n\rho \mathbf{g} + \bigtriangledown \cdot \mathbf{f} - \frac{\mu n^2}{k_p}\mathbf{U} \tag{1}$$

where t is time, n is the solid skeleton porosity, ρ is the water density, $\mathbf{U}$ is the velocity vector, $\mathbf{g}$ is the gravitational acceleration, μ is the total viscosity, and $\mathbf{f}$ is the stress tensor described by Newton's viscosity law, and k_p is the porous medium permeability given by the Kozeny Carman equation only applicable to laminar flow (Marshall, 1958),

$$\mathbf{f} = n\mu[\bigtriangledown \mathbf{U} + (\bigtriangledown \mathbf{U})^T] - np\mathbf{I}; \qquad k_p = \frac{1}{C_s T_0^3 S_s^2}\frac{n^3}{(1-n)^2}, \tag{2}$$

where T indicates the matrix transpose operation, p is the pore pressure, $\mathbf{I}$ is the identity matrix, C_s is the pore shape factor, T_0 is the tortuosity, and S_s is the specific surface area. Equation (2) employs a first-order closure principle for the total shear stress component, that is, $\tau = -\mu \mathrm{d}u/\mathrm{d}z$. For stationary and planar-homogeneous flow, the combined continuity and momentum equations reduce to

$$n\mu \frac{\mathrm{d}^2 u}{\mathrm{d}z^2} - \frac{\mu n^2}{k_p}u + n\rho g \sin\theta = 0, \tag{3}$$

where $u(z)$ is the sought mean velocity profile along x and θ is the slope angle of the wetland bed. It is to be noted that the assumptions employed here reduce Biot's law to the so-called Brinkman equation (Brinkman, 1949) used in prior porous media studies (Battiato & Rubol, 2014; Rubol et al., 2016, 2018.) To apply equation (3) to the FTW flow, the total viscosity term μ must be amended by adding a momentum dispersivity component L_{zz} (Battiato & Rubol, 2014; Fried & Combarnous, 1971) so that $\mu = \mu_v + L_{zz}$ with μ_v now being the dynamic viscosity of water (Wang & Chen, 2017; Zeng & Chen, 2011). Equation (3) frames the governing equation for the FTW, where $n = 1$ in the vegetation-free zone and $n \in (0, 1)$ for the canopy layer.

2.2. Analytical Solution for the Canopy Layer

As earlier noted, wind-induced stresses at the air-water interface are neglected so that the total stress at $z = H$ can be ignored. Moreover, the mean flow is assumed to be continuous at the bottom of the vegetation layer. These approximations yield the following boundary conditions to equation (3):

$$u(z)|_{z=h} = u_i; \qquad \frac{\mathrm{d}u(z)}{\mathrm{d}z}|_{z=H} = 0, \tag{4}$$

where u_i is the velocity located at the plane $z = h$, which is to be determined from momentum transport considerations in the inner layer. This mean velocity continuity condition has been used in prior studies dealing with an interface between the canopy top and a canopy-free zone as encountered in conventional canopy turbulence studies (Ghisalberti & Nepf, 2004; Nepf, 2012; Poggi et al., 2009; Yang et al., 2015). Moreover, numerous canopy flow experiments in both terrestrial and aquatic environments as well as flow over porous beds support a mean velocity continuity condition (Katul et al., 2004; Manes et al., 2011; Poggi, Porporato et al. 2004; Poggi, Katul & Albertson 2004; Raupach et al., 1996). To explore the general features of equation (3), three dimensionless parameters are now introduced

$$\xi = \frac{z}{h} \qquad \psi = \frac{u}{u_c} \qquad \Psi = \frac{u}{u_{*b}}, \tag{5}$$

where a characteristic velocity u_c in the canopy layer is defined as

$$u_c = \frac{h^2}{n(\mu_v + L_{zz})}\rho g \sin(\theta). \tag{6}$$

The choice of two velocity scales (ψ, Ψ) is to delineate the flow properties in the canopy layer (ψ) from the inner layer (Ψ) discussed later on. After normalization, the governing equation and boundary conditions are

$$\frac{\mathrm{d}^2\psi}{\mathrm{d}\xi^2} - \phi^2\psi + 1 = 0, \tag{7}$$

$$\psi(\xi)|_{\xi=1} = \psi_i \qquad \frac{\mathrm{d}\psi(\xi)}{\mathrm{d}\xi}|_{\xi=H/h} = 0, \tag{8}$$

where the porous resistivity coefficient ϕ is now defined as

$$\phi = \sqrt{\frac{n(H-h)^2}{k_p}} = S_s(H-h)\left(\frac{1}{n} - 1\right)\sqrt{C_s T_0^3}. \tag{9}$$

Thus solving equation (7) subject to these two boundary conditions yields the dimensionless mean velocity profile for the canopy layer $\xi \in (1, H/h)$,

$$\psi(\xi) = \left(\psi_i - \frac{1}{\phi^2}\right)\frac{\cosh[\phi(H/h - \xi)]}{\cosh[\phi(H/h - 1)]} + \frac{1}{\phi^2}, \tag{10}$$

where the dimensionless interfacial velocity $\psi_i = \psi(1)$ is to be determined from flow considerations in the inner or vegetation-free layer. The dimensionless water surface velocity $\psi_s(H/h)$ is given by

$$\psi_s = (\psi_i - \phi^{-2})\cosh[\phi(H/h - 1)]^{-1} + \phi^{-2}. \tag{11}$$

The dimensionless mean velocity profiles in equations (10) and (11) are shown in Figure 2 for varying porous resistivity in the vegetation zone.

Figure 2 shows that with increasing porous resistivity, the dimensionless velocity profile is reduced and approaches a Darcy-like flow $\psi(\xi) = u(z)/u_c \approx [(k_p/n)\rho g \sin(\theta)]/u_c = \text{constant}$. The normalized turbulent shear stress $(\Gamma(\xi) = (\mu_v + L_{zz})\mathrm{d}\psi/\mathrm{d}\xi)$ in the canopy layer, $\xi \in (1, H/h)$, can be determined as,

$$\Gamma(\xi) = \phi^{-1}(\mu + L_{zz})(1 - \psi_i\phi^2)\frac{\cosh\left[\phi(H/h - 1)\right]}{\sinh\left[\phi\,(H/h - \xi)\right]}. \tag{12}$$

The dimensionless shear stress profile is also shown in Figure 2. Deep inside the canopy $\xi \in (1 + \delta/h, H/h)$, the shear stress featured in Figure 2 is much smaller than the penetration height region $\xi \in (1, 1 + \delta/h)$. This is consistent with prior experiments (Ghisalberti, 2009; Nepf & Vivoni, 2000) illustrating that turbulent mixing mainly occurs around the canopy-water interfacial regions for dense canopies. It also demonstrates that as ϕ increases, the shear stress decreases toward the air-water interface as expected, because the stress

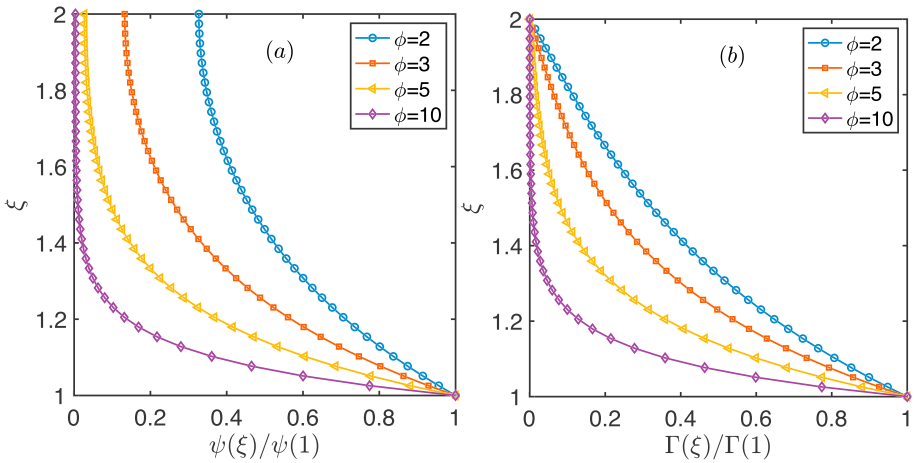

Figure 2. Analytical results for the canopy layer. (a) The dimensionless mean velocity profile as a function of dimensionless height $\xi = z/h$. The mean velocity is normalized by the interfacial velocity $\psi(1) = \psi_i$. (b) The dimensionless shear stress $\Gamma(\xi)/\Gamma(1)$ profile as a function of dimensionless height, where $\Gamma(1)$ is the interfacial shear stress. Note the dependence on porous resistivity coefficient ϕ in the canopy layer.

is forced to zero at the interface. In submerged canopy flows, a penetration depth is commonly defined as the plane at which the shear stress decreases to some 10% (Nepf & Vivoni, 2000; Ghisalberti, 2009) of its maximum. Consistent with this definition, a similar penetration height (δ) for the suspended canopy is now introduced. The δ is defined here by the length from the canopy bottom to where the shear stress decreases up to 10% of the maximum shear stress at the location $\Gamma_{\max} = \Gamma(1)$. Using this definition, the penetration height can be directly determined from equation (12) as

$$\delta = H - h\left[\phi^{-1}\sinh^{-1}\left(p\sinh\left(\phi\left(\frac{H}{h}-1\right)\right)\right)+1\right], \tag{13}$$

where $p = 10\%$ is the stress reduction from its maximum. Equation (13) indicates that the penetration height is determined from the canopy length and the porous resistivity of the canopy layer. This dependence of δ on the porous resistivity coefficient ϕ is shown in Figure 3.

Larger porous resistivity prohibits some fluid from penetrating into the porous media (i.e., inside the suspended canopy). Hence, as expected from logical considerations, the penetration height must decrease with increasing ϕ as shown in Figure 3.

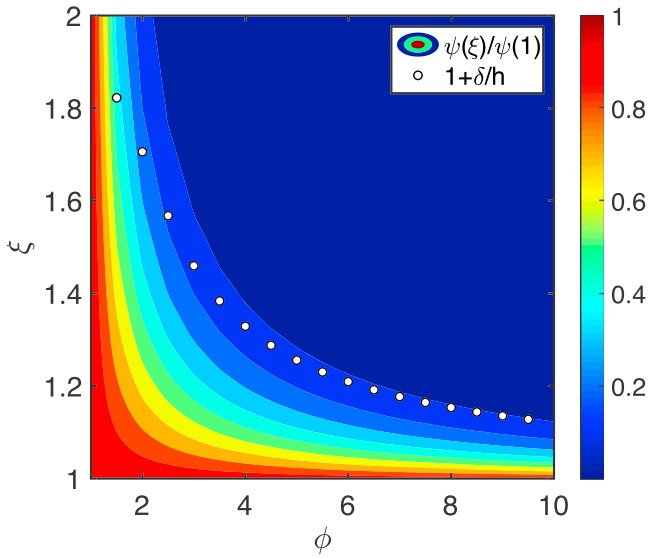

Figure 3. Dependence of the penetration depth δ on the porous resistivity coefficient ϕ in the canopy layer.

2.3. Analytical Solution for the Inner Layer

In the inner layer or vegetation free zone, the governing mean momentum equation reduces to a balance between the gravitational driving force and the total stress gradient (i.e., $g\sin(\theta) + \mathrm{d}\tau/\mathrm{d}z = 0$) as common to uniform and steady flow in wide channels. What makes the flow in the inner layer different from conventional open channel flows is the influence of the suspended canopy (Huai et al., 2012; Li et al., 2015). As noted earlier, the inner layer is subjected to two forms of stresses arising from the canopy medium and the channel bed, respectively. In wide open channel flows, the turbulent stress at the water surface is zero so that the total bed stress and water depth dictate the entire stress profile. When the top and bed stresses are different (and even opposite) as may occur in the presence of another bounding surface (e.g., ice sheets, water lily leaves), the stress distribution is labeled asymmetric. For such asymmetric stress distribution, prior studies (Huai et al., 2012) separated this layer into two parts at the location of maximum velocity, which was assumed to be a free shear-stress surface. The mean velocity profiles were then fitted with two modified log-laws as if the upper and lower boundaries impose independent canonical turbulent boundary layers. The resulting mean velocity gradient appears discontinuous at the location of maximum velocity (Han et al., 2018). Since the interest here is not in all the details of the mean velocity within the inner layer but a link between the inner and canopy layers, an integral treatment for the inner layer is considered. Integrating the mean momentum balance equation must lead to a linear stress profile given by $\tau = \tau_b(1-\xi)$, where τ_b is the bed shear stress. The link is now achieved by noting that the inner layer is subjected to two bounding shear stresses (τ_v and τ_b). The only expression that can satisfy these two boundary conditions while maintaining linearity in the stress profile is

$$\tau = \tau_b - (\tau_v + \tau_b)\xi = \tau_b[1 - (1 + \lambda^2)\xi]. \tag{14}$$

Equation (14) includes both stresses through $\lambda = \sqrt{\tau_v/\tau_b}$ and remains consistent with prior results for asymmetric shear stress conditions (Guo et al., 2017; Han et al., 2018; Teal et al., 1994). The maximum mean velocity is expected to occur at the point where the mean velocity gradient is zero or $\tau = 0$, that is,

$$\xi_m = \frac{1}{1 + \lambda^2}, \tag{15}$$

where ξ_m is the point where the mean velocity attains a maximum value in the inner layer. It is evident that when $\lambda > 1$, $\xi_m < 1/2$, implying that the location of the maximum velocity is closer to the suspended canopy bottom. Moreover, if $\lambda = 1$, equation (14) reduces to the canonical pipe flow case (symmetric flow), where the top and bottom shear stresses are equal. For open channel flows, the top shear stress is negligible and $\lambda = 0$ so that $\xi_m = 1$ (maximum velocity at the free water surface). Asymmetric flow conditions necessitate $\lambda \neq 1$. Combining ξ_m with equation (14), the turbulent shear stress distribution can be expressed as

$$\tau = \tau_b \left(1 - \frac{\xi}{\xi_m}\right). \tag{16}$$

Using first-order closure principle (Guo, 2017; Guo et al., 2017; Hultmark et al., 2012, 2013; Katul et al., 2004; Poggi, Porporato et al. 2004), the turbulent shear stress can be modeled with $\tau = \mu' \mathrm{d}u/\mathrm{d}z$, where μ' is a turbulent dynamic eddy viscosity that must be determined to recover the aforementioned stress profile. Building on prior work for such asymmetric flows (Guo et al., 2017), an amended eddy viscosity model is now proposed by introducing a channel permeability coefficient β_1 and is given by

$$\mu' = \kappa h u_{*b} \left(\beta_1 - 2\xi\right) \beta_2 \xi \left[\alpha\left(\frac{\xi}{\xi_\beta} - 1\right)^2 + 1\right], \tag{17}$$

where $\kappa = 0.41$ is the von Karman constant, β_1 is a coefficient proposed here to reflect the permeability of the vegetation layer. This coefficient can be determined from continuity and smoothness considerations of the local velocity at the water-vegetation interface. Theoretically, β_1 can be derived from the velocity smoothness condition $\mathrm{d}\psi(\xi)/\mathrm{d}\xi|_{1+} = \mathrm{d}\psi(\xi)/\mathrm{d}\xi|_{1-}$ as discussed later. It is noted here that when $\beta_1 = 2$, Equation (17) recovers the eddy viscosity model earlier proposed for ice-covered flow (Guo et al., 2017). The other coefficients are expressed as

$$\alpha = \frac{1-\lambda}{\lambda - \lambda^{2n}} \quad \beta_2 = \frac{1}{\beta_1}\frac{\lambda - \lambda^{2n}}{1-\lambda^{2n}} \quad \xi_\beta = \frac{\beta_1}{2(1+\lambda^n)}, \tag{18}$$

where $n = 5/6$ is derived from considerations discussed elsewhere (Guo et al., 2017). Inserting these coefficients into equation (16), recalling the definition of the normalized mean velocity for the inner layer ($\Psi = u/u_{*_b}$), the normalized mean velocity gradient is now given as

$$\frac{\mathrm{d}\Psi}{\mathrm{d}\xi} = \frac{1}{\kappa}\left[\frac{1}{2\xi} + \frac{\lambda}{2\xi - 2} + \frac{1+\lambda}{2\xi_\beta}\frac{\xi/\xi_\beta - 1}{(\xi/\xi_\beta - 1)^2 + 1/\alpha} + \frac{1}{2}\frac{(1-\lambda^{n+1})(1+\lambda^n)}{(\xi/\xi_\beta - 1)^2 + 1/\alpha}\right]. \tag{19}$$

Integrating equation (19) from ξ_β to any depth ξ with a pseudo-known condition $\Psi(\xi_\beta) = \Psi_\beta$ yields the mean velocity shape given by

$$\begin{aligned}\kappa\Psi(\xi) = \kappa\Psi_\beta + \ln\left(\frac{\xi}{\xi_\beta}\right) + \lambda\ln\left(\frac{\beta_1 - 2\eta}{\beta_1 - 2\lambda_c}\right) - \frac{1+\lambda}{\beta_1}\ln\left[1 + \alpha\left(1 - \frac{\xi}{\xi_\beta}\right)^2\right] \\ - \left(1-\lambda^{n+1}\right)\sqrt{\alpha}\tan^{-1}\left[\sqrt{\alpha}\left(1 - \frac{\xi}{\xi_\beta}\right)\right].\end{aligned} \tag{20}$$

Combining equation (15) with equation (20), the maximum normalized mean velocity at the point $\xi = \xi_m$ can be evaluated as

$$\begin{aligned}\kappa\Psi_m = \kappa\Psi_\beta + \ln\left(\frac{\xi_m}{\xi_\beta}\right) + \lambda\ln\left(\frac{\beta_1 - 2\xi_m}{\beta_1 - 2\xi_\beta}\right) - \frac{1+\lambda}{\beta_1}\ln\left[1 + \alpha\left(1 - \frac{\xi_m}{\xi_\beta}\right)^2\right] \\ - \left(1-\lambda^{n+1}\right)\sqrt{\alpha}\tan^{-1}\left[\sqrt{\alpha}\left(1 - \frac{\xi}{\xi_\beta}\right)\right].\end{aligned} \tag{21}$$

Comparing equations (20) and (21), the solution for the asymmetric layer ($\xi \in (0,1)$) is given as

$$\begin{aligned}\kappa\Psi(\xi) = \kappa\Psi_m - \ln\left(\frac{\xi_m}{\xi}\right) + \lambda\ln\left(\frac{\beta_1 - 2\xi_m}{\beta_1 - 2\xi}\right) - \frac{1+\lambda}{\beta_1}\ln\left[\frac{(\xi_m - \xi_\beta)^2 + \xi_\beta^2}{\alpha(\xi - \xi_\beta)^2 + \xi_\beta^2}\right] \\ - \left(1-\lambda^{n+1}\right)\sqrt{\alpha}\tan^{-1}\left[\frac{\sqrt{\alpha}\xi_\beta(\xi_m - \xi_\beta)}{\xi_\beta^2 + \alpha(\xi - \xi_\beta)(\xi_m - \xi_\beta)}\right].\end{aligned} \tag{22}$$

The normalized turbulent shear stress ($\Gamma(\xi) = \mu\mathrm{d}\Psi/\mathrm{d}\xi$) in the inner layer for $\xi \in (0,1)$ is

$$\Gamma(\xi) = (\beta_1 - 2\xi)\beta_2\xi\left[\alpha\left(\frac{\xi}{\xi_\beta} - 1\right)^2 + 1\right]\Gamma_v(\xi) \tag{23}$$

with

$$\Gamma_*(\xi) = \frac{1}{\kappa}\left[\frac{1}{2\xi} + \frac{\lambda}{2\xi - 2} + \frac{1+\lambda}{2\xi_\beta}\frac{\xi/\xi_\beta - 1}{(\xi/\xi_\beta - 1)^2 + 1/\alpha} + \frac{1}{2}\frac{(1-\lambda^{n+1})(1+\lambda^n)}{(\xi/\xi_\beta - 1)^2 + 1/\alpha}\right] \tag{24}$$

Substituting equation (12) into equation (23), the expression for β_1 can be derived as

$$\beta_1 = \frac{(\mu + L_{zz})(1 - \psi_i\phi^2)}{\phi\cosh[\phi(H/h - 1)]}\frac{\sinh[\phi(H/h - 1)]}{\beta_2[\alpha(1/\xi_\beta - 1)^2 + 1]\Gamma_*(1)} + 2. \tag{25}$$

It is to be noted the expression derived here ensures that $\beta_1 \geq 2$. The sought interfacial velocity between the inner and canopy layers can now be determined at $\psi_i = \psi(1)$ for $\xi = 1$ as

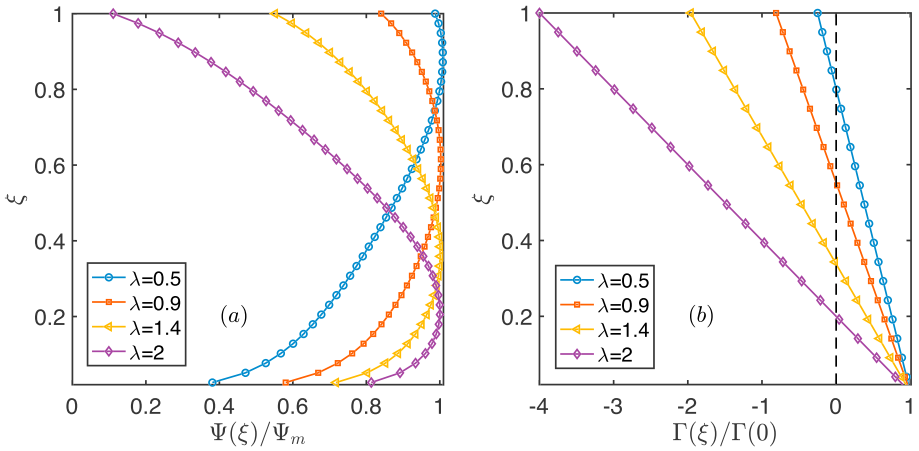

Figure 4. Model results for the inner (vegetation-free) asymmetric layer. (a) The dimensionless mean velocity profile Ψ is plotted as a function of dimensionless height $\xi = z/h$ in the inner layer for various λ values. Each mean velocity is normalized by the maximum velocity Ψ_m. (b) The dimensionless shear stress is shown as a function of dimensionless height $\xi = z/h$ in the inner layer for various λ values. Each shear stress is normalized by the bottom shear stress $\Gamma(0)$. The (linear) stress profile crosses zero at ξ_m.

$$\kappa\psi_i = \kappa\Psi_m - \ln\left(\xi_m\right) + \lambda\ln\left(\frac{\beta_1 - 2\xi_m}{\beta_1 - 2}\right) - \frac{1+\lambda}{\beta_1}\ln\left[\frac{\left(\xi_m - \xi_\beta\right)^2 + \xi_\beta^2}{\alpha\left(\xi - \xi_\beta\right)^2 + \xi_\beta^2}\right]$$
$$- \left(1 - \lambda^{n+1}\right)\sqrt{\alpha}\tan^{-1}\left[\frac{\sqrt{\alpha}\xi_\beta\left(\xi_m - \xi_\beta\right)}{\xi_\beta^2 - \alpha\xi_\beta\left(\xi_m - \xi_\beta\right)}\right]. \quad (26)$$

Equation (22) admits a zero shear stress at $\xi = \xi_m$ as before. Furthermore, the bottom and top roughness height are not required for the velocity and shear stress determination in the canopy layer, where these factors are packed into one parameter ($=\lambda$). To summarize, equations (22) and (10) form a coupled transport model for the FTW. In the canopy or porous media layer, the overall drag is confined to one porous resistivity coefficient, ϕ. The differing roughness questions are addressed with another asymmetric property parameter, λ. The influence of λ on the mean velocity profile is shown in Figures 4.

Figure 4 shows that the mean velocity profile is sensitive to λ. When $\lambda < 1$, the channel bed roughness is more significant in shaping the mean velocity profile, at least when compared with the canopy top. As expected, the location of the maximum velocity is closer to the canopy bed. For completeness, Figure 4 also shows the concomitant total stress profile (linear in all cases) up to the point when $\tau = \tau_v$ (i.e., ξ_v). Unsurprisingly, the point at which $\tau = 0$ and Ψ is maximum are colocated at $\xi_m = (1+\lambda^2)^{-1}$.

3. Comparisons With Experiments

The model is now compared with experiments on suspended canopy flow reported by Plew (2010) and Han et al. (2018). Since Plew (2010) used rigid rods to represent the suspended vegetation, all their seven reported runs are used in this comparison. Han et al. (2018) employed artificial lotus leaves to represent a canopy-covered flow, which still generates shear stress asymmetry resembling the inner layer of the FTW here. The conditions for the data from Plew (2010) (notated with the initial "B") and Han et al. (2018) (represented with the initial "R") are summarized in Table 1. The experiments do not report ϕ and λ, and they do not provide sufficient details to infer them independent of the model here. Hence, these two variables were used as fitting parameters in the comparison between model and measurements. All the dimensional parameters reported in the table and figures are in the international system of units.

The data used include mean velocity and shear stress profiles and bulk mean velocities. Compared with prior semianalytical models (Huthoff et al., 2007; Konings et al., 2012) and prior analytical work (Battiato & Rubol, 2014), the present model requires the specification of two parameters (ϕ and λ). Hence, the "degrees of freedom" here is commensurate with prior models that require a local drag coefficient and a mixing length

Table 1
Summary of the Published Experimental Conditions and Relevant Parameters Computed by Us When Fitting the Proposed Model to the Experiments (ϕ and λ)

Run	H	h	a	$g\sin(\theta)$	U	V	δ_e	ϕ	λ	β_1
B2	0.2	0.025	1.272	0.001470	0.0876	0.0567	0.0314	1.83	2.01	7.2
B5	0.2	0.050	1.272	0.001170	0.0841	0.0580	0.0342	5.62	2.57	8.5
B9	0.2	0.075	1.272	0.001460	0.0843	0.0566	0.0252	6.85	1.72	3.2
B12	0.2	0.100	1.908	0.001978	0.0876	0.0604	0.0445	5.17	1.75	2.9
B13	0.2	0.100	1.272	0.001528	0.0841	0.0616	0.0410	5.62	2.68	7.3
B14	0.2	0.100	0.954	0.001009	0.0843	0.0658	0.0372	6.18	2.18	5.3
B15	0.2	0.100	0.477	0.000489	0.0855	0.0752	0.0521	4.39	2.23	6.9
R1	0.18	0.18	NA	0.004	0.0938	NA	NA	NA	0.91	2.0
R2	0.19	0.19	NA	0.005	0.1051	NA	NA	NA	0.90	2.0

*Note.*The β_1 presented here is an inferred quantity derived from the smoothness condition at the interface between the canopy and inner layers. The plausibility of the obtained values is discussed separately. The length scales (H, h, δ_e) are in m, a is in m^{-1}, g is in m/s^2, and the velocity scales (U, V) are in m/s.

(Poggi et al., 2009; Huai et al., 2012) or a single fitting parameter that includes both the drag coefficient and the mixing length scale discussed elsewhere (Battiato & Rubol, 2014).

3.1. Velocity Distribution

The model is now evaluated for the inner and canopy layers. The model parameters in equations (10) and (22) for each run were determined from the data as follows. For the inner layer, Ψ_m can be directly obtained from data by using spline interpolation or other smoothing methods as discussed elsewhere (Guo, 2017; Guo et al., 2017). Next, λ is fitted to data using a least squares minimization method. After inferring λ, the interfacial velocity u_i or ψ_i are determined by setting $\xi = 1$ in equation (22). We also use least squares method to fit ϕ to data using equation (10) inside the canopy as no other information about the properties of the porous medium are provided. A list of the fitted (and derived) parameters for each run in the experiments is presented in Table 1.

Figure 5 shows that the proposed two-domain model can describe the mean velocity profile for both—the canopy and the inner layers when compared to experiments (Plew, 2010). It is noted that the mean velocity in the inner layer is not logarithmic. This finding demonstrates the "roughness bed" generated by the bottom of the suspended canopy is significant in shaping the mean velocity profile. In the canopy layer, the mean

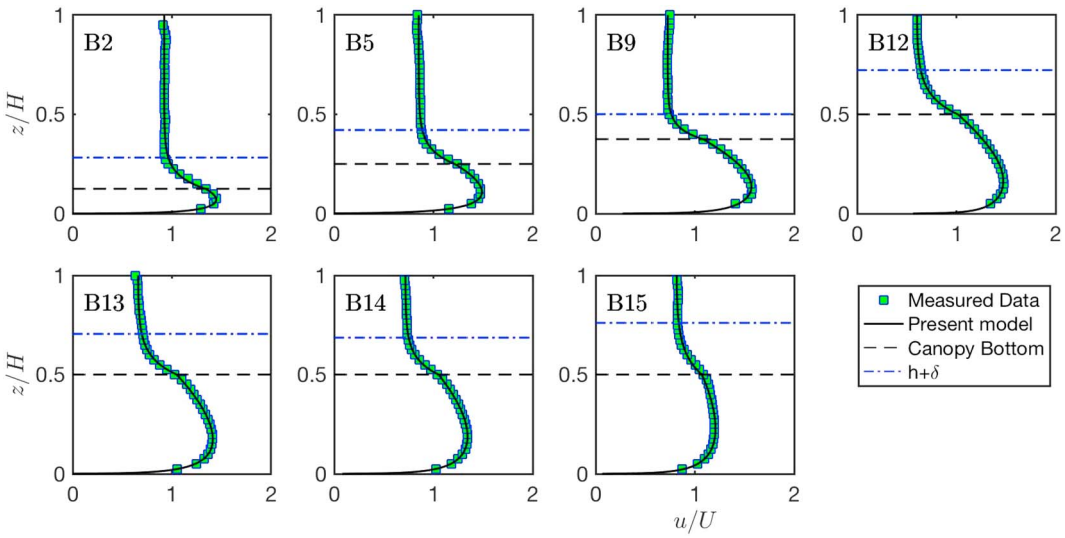

Figure 5. Measured and fitted mean velocity profiles for the suspended canopy flow represented by rigid rods. B2 to B15 are the original data points reported by Plew (2010). The ratio of the canopy height to the flow depth varies from 0.125 to 0.5 as shown in the blue dash-dotted lines.

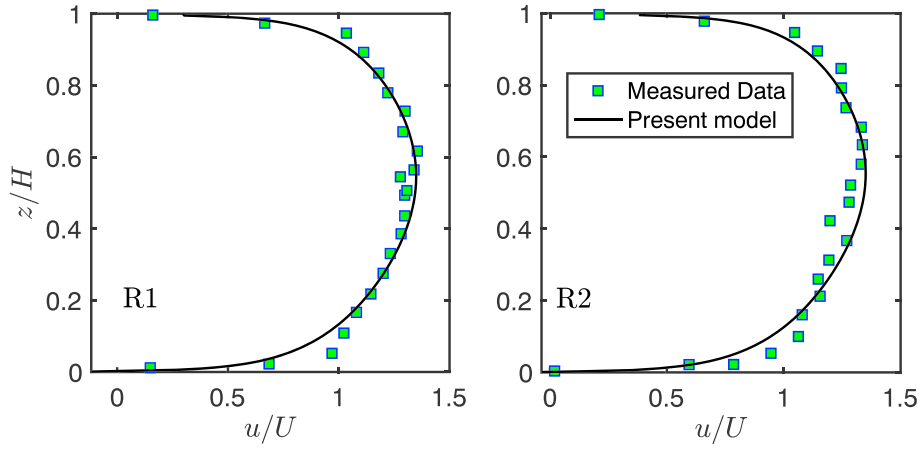

Figure 6. Measured and modeled mean velocity profiles for the suspended canopy flow with lotus leaves at the top. R1 (left) and R2 (right) are the original data points reported by Han et al. (2018).

velocity is not uniform along the z direction (as expected from Darcy's equation). The effective porosity determined here for the suspended canopy is far larger than typical soil porosity, where Biot's Law (Zhao et al., 2012) was initially proposed. Although the canopy is not strictly a porous medium, Figure 5 shows that the proposed equation (10) can reproduce the mean velocity profiles inside the canopy layer for a wide range of flow and canopy conditions.

Figure 6 compares data from Han et al. (2018) with equation (10), where λ is near unity for these two runs. This choice of λ is due to the near impermeability of the lotus leaves, which form a vegetated cover on the water surface. The vegetated cover is similar to ice cover in terms of roughness effect. With $\lambda = 1$, equation (10) simplifies to the classical symmetric pipe flow case.

3.2. Shear Stress Profile

The shear stress profiles for the canopy flow case are also fitted seperately by following the similar procedures as described in the prior velocity section, and shown in Figure 7. The total linear shear stress profiles predicted from equations (12) and (14) are compared with the observed turbulent shear stress data reported by Plew (2010). Figure 7 shows that the two-domain approach recovers the shear stresses in both layers. However, it is to be noted that the shear stress profile in Figure 7 is not absolutely continual at the interface between the canopy layer and the inner water layer, since the shear stress is fitted for the canopy layer and

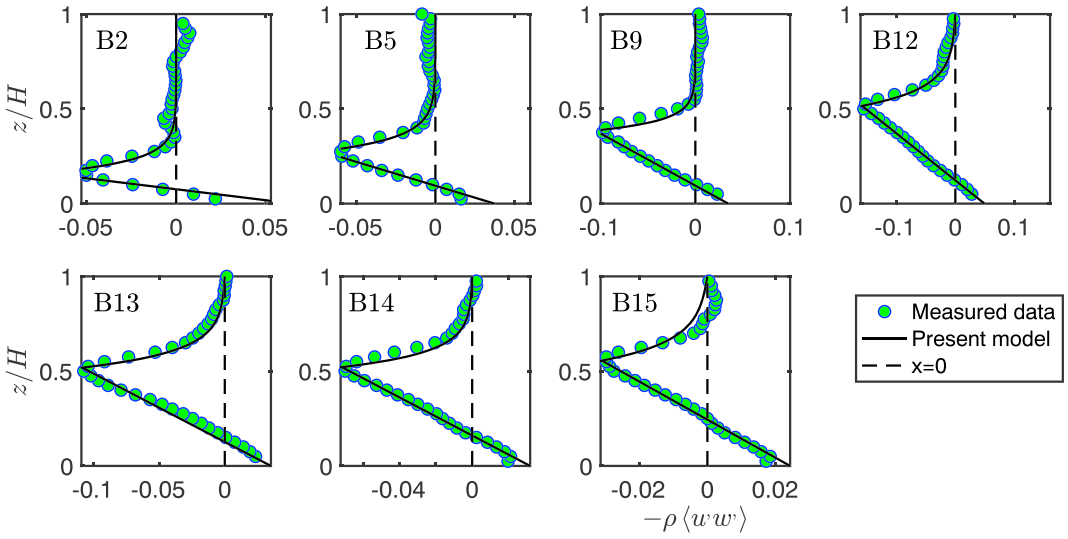

Figure 7. Comparison between measured and modeled shear stress profiles for the suspended canopy flow assuming $\lambda = 1$. The shear stress scale $\rho\langle u'w'\rangle$ is in kg·m^{-1}·s^{-2}.

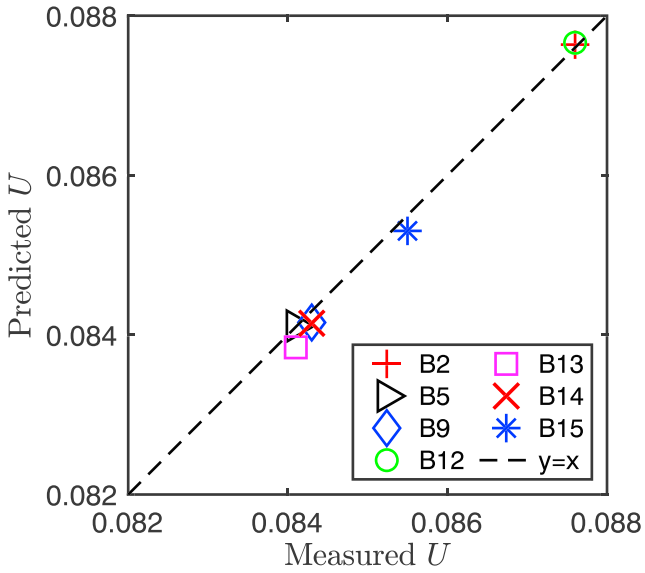

Figure 8. Comparison between measured and modeled bulk velocity. The dashed line is the one-to-one agreement and the velocity scale (U) is in m/s.

the inner water layer seperately (this is a flaw of the asymmetric method as stated by Guo et al., 2017) to optimize the calculation efficiency. The shear stress in the canopy layer decreases rapidly in the subrange ($z \in (h+\delta, H)$). This finding suggests that turbulent mixing is confined to $(h, h+\delta)$ inside the vegetation, which agrees with other canopy flow experiments (Ghisalberti & Nepf, 2004; Nepf & Vivoni, 2000). In the inner layer beneath the canopy, the shear stress linearly varies with z as expected. In the cases studied here, the top shear stress is much larger than the channel bed shear stress.

3.3. Bulk Velocity

Finally, the predicted bulk (or depth-averaged) velocity is compared with measurements. Figure 8 compares predicted bulk velocity derived by integrating equations (10) and (22) from $z = 0$ to $z = H$ with measured ones from Plew (2010). Figure 8 shows that the predicted bulk velocity values match the measurements reasonably.

4. Discussion and Model Limitation

One of the key simplifying assumptions used here is approximating the flow within the vegetated layer of FTWs as a porous medium described by the Brinkman equation (Brinkman, 1949). This assumption is plausible given that the Brinkman equation to which the model essentially reduces to is valid for highly permeable porous media (Auriault, 2009). As shown in prior studies (Ling et al., 2018), the Brinkman equation can be used when the porous media is of high porosity. The associated porous resistivity coefficient ϕ packs all the morphological geometry of the vegetation patches. This representation does not require separate treatment of each individual canopy stem and is operational when considering distributions of particle retention times in FTWs (Clark, 2011; Khan et al., 2013). In reality, suspended canopies exist in many forms including cages, rafts, and some kelp, and their morphology can deviate appreciably from a dense porous medium where Biot's or Brinkman's equation applies. Furthermore, the influence of surface wind under different meteorological conditions will contribute to the generation of surface waves and surface stresses not considered here. Density stratification has been ignored and those effects can lead to porous-media convective transport as well. Perhaps most restrictive is the fact that the model focused on planar-homogeneous and stationary flow conditions, which are likely to be violated in practice due to nonuniformity in vegetation growth, channel slope, channel roughness, transients in meteorological drivers, and nonsteadiness in the inflow hydrograph to the FTW. Nonetheless, these idealized conditions must be first understood and described before more complex situations are considered.

When adopting all the aforementioned assumptions, the mean velocity profile emerging from the proposed model is not uniform and deviates from Darcy's equation or some modification to it. This deviation is not

surprising as the roughness effect arising from the canopy bottom may be related to Kelvin-Helmholtz instabilities (Finnigan, 2000; Nepf, 2012; Poggi et al., 2009; Raupach et al., 1996) or to large-scale eddies penetrating the porous elements (Manes et al., 2012). When adopting this representation for the canopy, the mean velocity profile inside the canopy layer is dependent on the vegetation density through a parameter ϕ. When ϕ is large, Biot's law converges to Darcy's law and conventional porous media equations for laminar flow are recovered. However, if ϕ is small, Biot's law yields large deviations from Darcy's law but is expected to converge to Stokes equation due to the effective viscosity introduced by the turbulent part and employed in Biot's law or the Brinkman equation (Brinkman, 1949). The inner or vegetation-free water layer exhibits an asymmetric shear stress profile that remains linear with depth in the absence of any obstructions. Hence, an integral representation can be used provided the effect of such stress asymmetry is accounted for in a newly proposed eddy viscosity formulation. The proposed approach predicts the location of maximum local velocity as a function of a shear stress index λ in the vegetation-free zone. This index is intrinsically a ratio of two roughness effects due to the channel bed and the auxiliary canopy bed. Once these properties are predetermined from data or other models, the solution to the inner layer can be completed. A "blue print" of how λ may be inferred separately is briefly discussed.

The dimensionless shear stress index was defined as $\lambda^2 = \tau_v/\tau_b$ and reflects the asymmetric effects of the two boundary conditions on the stress profile. Because the physical mechanisms shaping τ_v resemble those of flow over porous gravel beds, the section here explores the possibility of inferring λ from the properties of the porous bed. The approach is guided by the phenomenological model of Manes et al. (2012) that considered the turbulent shear stress over a permeable boundary as consisting of two parts: $\tau = \tau_o + \tau_a$, where τ_o is the commonly-mentioned shear stress formulated over small-roughness boundary (or solid boundary), and τ_a is an additional shear stress emerging from the turbulent momentum exchange due to large-scale turbulent eddies penetrating the porous medium. For the highly permeable case, the work of Manes et al. (2012) has shown that $\tau_a \gg \tau_o$. If the turbulent shear stress near the canopy bottom is approximated by the shear stress due to large-scale roughness (Li et al., 2019) only, then $\tau_v = \tau_a$. The τ_a can be derived using the published model of Manes et al. (2012). In this model, τ_a accounts for the Forchheimer corrections to Darcy's law as well as the permeability of the medium. For the shear stress formulated over the channel bed, only the small-size eddies are assumed to transport momentum and $\tau_b = \tau_o$. Hence, the dimensionless stress index can be modeled as $\lambda \approx \tau_a/\tau_o$. For τ_o, the phenomenological model of Gioia and Chakraborty (2006) (hereinafter GC06) applicable to a solid wall can be employed. At high Reynolds number, GC06 describes $\tau_o = \rho\kappa_t u_s U$, where κ_t is a constant coefficient of order unity, U is the bulk mean velocity of the entire inner layer and u_s is a characteristic turn-over velocity of an eddy of size s transporting momentum within the roughness elements characterized by size r. Using the arguments in GC06 for rough boundary layer flows,

$$u_s \sim U(r/H)^{1/3}. \tag{27}$$

A review of roughness-induced friction factor for open flows over vegetated channels and highly permeable boundaries can be found elsewhere (Cheng, 2011; Manes et al., 2012) and are not repeated here. However, the usage of GC06 and the phenomenological model of Manes et al. (2012) allow independent determination of λ from the roughness properties of the bed and the porous media properties of the vegetation if they are a priori known.

5. Summary and Conclusion

FTWs are an emerging phytoremediation technique introduced in recent years for stormwater treatment. For these techniques to be integrated into water treatment design options, models for describing the hydrodynamics within FTWs are necessary (but not sufficient). Developing such models remains a formidable challenge and motivated the proposed work here. A coupled two-domain model is proposed for a simplified FTW. The proposed model is minimal and must be viewed as an embryonic step toward advancing flow and transport in FTW. The initial focus is necessarily biased toward processes common to all FTWs: a vegetation layer and a vegetation-free layer in a sloping channel.

The vegetation layer is modeled as a porous medium where Biot's (or Brinkman's) law is assumed to apply. The momentum equation in the streamwise direction is then solved after amending the fluid viscosity with a momentum dispersivity coefficient that is needed to bridge the bottom boundary condition of the vegetated zone to the aforementioned porous media equations. Turbulent mixing is intense inside the penetrated

canopy region near this boundary; that is, $z \in (h, h + \delta)$. Similar to prior work on flow over submerged canopies (Battiato & Rubol, 2014; Papke & Battiato, 2013), the proposed model also provides a direct expression for the penetration depth from this aforementioned boundary. However, as a point of departure from other prior semianalytical submerged vegetated flow models (Huthoff et al., 2007; Konings et al., 2012), the work here does not require explicitly a drag coefficient and a leaf area density. These coefficients are combined into one porous resistivity coefficient ϕ, which can be predetermined from the vegetation configuration. The shear stress distribution within the inner layer (or vegetation-free zone) is highly asymmetric. Drawing on analogies to similar asymmetric flow configurations, an augmented eddy viscosity is proposed that accommodates such stress asymmetry. The parameter λ describing the stress asymmetry is needed and shown to be related to the vegetation and channel properties with the aid of two recent phenomenological models presented elsewhere (Gioia & Chakraborty, 2006; Manes et al., 2012). The proposed model reproduced all the complex patterns in the mean velocity and stress profiles published in laboratory studies when the two constants ϕ and λ are used as fitting parameters. Field testing of this model is a topic that is best kept for future effort.

Acknowledgments
We thank David Plew for sharing the data set used in the model evaluation, and Junke Guo for assisting with the codes for the asymmetric layer. All the data used in this work have been reported elsewhere (Han et al., 2018; Plew, 2010). G. K. acknowledges support from the U.S. National Science Foundation (NSF-EAR-1344703, NSF-AGS-1644382, and NSF-IOS-1754893). W. H. acknowledges the financial support from the Natural Science Foundation of China (51439007, 11172218, and 11372232).

References

Auriault, J.-L. (2009). On the domain of validity of Brinkmans equation. *Transport in Porous Media*, *79*(2), 215–223.
Battiato, I., & Rubol, S. (2014). Single-parameter model of vegetated aquatic flows. *Water Resources Research*, *50*, 6358–6369. https://doi.org/10.1002/2013WR015065
Biot, M. A. (1956). Theory of propagation of elastic waves in a fluid-saturated porous solid. II. Higher frequency range. *The Journal of the Acoustical Society of America*, *28*(2), 179–191.
Brinkman, H. (1949). A calculation of the viscous force exerted by a flowing fluid on a dense swarm of particles. *Flow, Turbulence and Combustion*, *1*(1), 27.
Cheng, N.-S. (2011). Representative roughness height of submerged vegetation. *Water Resources Research*, *47*, W08517. https://doi.org/10.1029/2011WR010590
Clark, M. M. (2011). *Transport modeling for environmental engineers and scientists*. New York: John Wiley & Sons.
de Stefani, G., Tocchetto, D., Salvato, M., & Borin, M. (2011). Performance of a floating treatment wetland for in-stream water amelioration in NE Italy. *Hydrobiologia*, *674*(1), 157–167.
Finnigan, J. (2000). Turbulence in plant canopies. *Annual Review of Fluid Mechanics*, *32*(1), 519–571.
Fried, J., & Combarnous, M. (1971). Dispersion in porous media, *Advances in hydroscience* (Vol. 7, pp. 169–282). Boulder: Elsevier.
Ghisalberti, M. (2009). Obstructed shear flows: Similarities across systems and scales. *Journal of Fluid Mechanics*, *641*, 51–61.
Ghisalberti, & Nepf (2004). The limited growth of vegetated shear layers. *Water Resources Research*, *40*, W07502. https://doi.org/10.1029/2003WR002776
Gioia, G., & Chakraborty, P. (2006). Turbulent friction in rough pipes and the energy spectrum of the phenomenological theory. *Physical Review Letters*, *96*(4), 044502.
Guo, J. (2017). Eddy viscosity and complete log-law for turbulent pipe flow at high Reynolds numbers. *Journal of Hydraulic Research*, *55*(1), 27–39.
Guo, J., Shan, H., Xu, H., Bai, Y., & Zhang, J. (2017). Exact solution for asymmetric turbulent channel flow with applications in ice-covered rivers. *Journal of Hydraulic Engineering*, *143*(10), 04017041.
Han, L., Zeng, Y., Chen, L., & Li, M. (2018). Modeling streamwise velocity and boundary shear stress of vegetation-covered flow. *Ecological Indicators*, *92*, 379–387.
Headley, T., Tanner, C. C., & Council, A. R. (2008). *Application of floating wetlands for enhanced for stormwater treatment: A review*. Auckland: Auckland Regional Council. http://www.aucklandcity.govt.nz/council/documents/technicalpublications/TP324-FloatingWetlandReview-Final.pdf
Hu, S.-Y., Chiueh, P.-T., & Hsieh, P.-C. (2014). A novel semi-analytical approach for non-uniform vegetated flows. *Advances in Water Resources*, *64*, 1–8.
Huai, W., Hu, Y., Zeng, Y., & Han, J. (2012). Velocity distribution for open channel flows with suspended vegetation. *Advances in Water Resources*, *49*, 56–61.
Hultmark, M., Vallikivi, M., Bailey, S., & Smits, A. (2012). Turbulent pipe flow at extreme Reynolds numbers. *Physical Review Letters*, *108*(9), 094501.
Hultmark, M., Vallikivi, M., Bailey, S., & Smits, A. (2013). Logarithmic scaling of turbulence in smooth-and rough-wall pipe flow. *Journal of Fluid Mechanics*, *728*, 376–395.
Huthoff, F., Augustijn, D., & Hulscher, S. J. (2007). Analytical solution of the depth-averaged flow velocity in case of submerged rigid cylindrical vegetation. *Water Resources Research*, *43*, W06413. https://doi.org/10.1029/2006WR005625
Katul, G. G., Mahrt, L., Poggi, D., & Sanz, C. (2004). One-and two-equation models for canopy turbulence. *Boundary-Layer Meteorology*, *113*(1), 81–109.
Khan, S., Melville, B. W., & Shamseldin, A. (2013). Design of storm-water retention ponds with floating treatment wetlands. *Journal of Environmental Engineering*, *139*(11), 1343–1349.
Konings, A. G., Katul, G. G., & Thompson, S. E. (2012). A phenomenological model for the flow resistance over submerged vegetation. *Water Resources Research*, *48*, W02522. https://doi.org/10.1029/2011WR011000
Leiva, A. M., Núñez, R., Gómez, G., López, D., & Vidal, G. (2018). Performance of ornamental plants in monoculture and polyculture horizontal subsurface flow constructed wetlands for treating wastewater. *Ecological Engineering*, *120*, 116–125.
Li, S., Huai, W., Cheng, N.-S., & Coco, G. (2019). Prediction of mean turbulent flow velocity in a permeable-walled pipe. *Journal of Hydrology*, *573*, 648–660.
Li, S., Shi, H., Xiong, Z., Huai, W., & Cheng, N. (2015). New formulation for the effective relative roughness height of open channel flows with submerged vegetation. *Advances in Water Resources*, *86*, 46–57.

Ling, B., Oostrom, M., Tartakovsky, A. M., & Battiato, I. (2018). Hydrodynamic dispersion in thin channels with micro-structured porous walls. *Physics of Fluids*, *30*(7), 076601.

Lowe, R. J., Shavit, U., Falter, J. L., Koseff, J. R., & Monismith, S. G. (2008). Modeling flow in coral communities with and without waves: A synthesis of porous media and canopy flow approaches. *Limnology and Oceanography*, *53*(6), 2668–2680.

Manes, C., Poggi, D., & Ridolfi, L. (2011). Turbulent boundary layers over permeable walls: Scaling and near-wall structure. *Journal of Fluid Mechanics*, *687*, 141–170.

Manes, C., Ridolfi, L., & Katul, G. (2012). A phenomenological model to describe turbulent friction in permeable-wall flows. *Geophysical Research Letters*, *39*, L14403. https://doi.org/10.1029/2012GL052369

Marshall, T. (1958). A relation between permeability and size distribution of pores. *European Journal of Soil Science*, *9*(1), 1–8.

Nepf (2012). Flow and transport in regions with aquatic vegetation. *Annual Review of Fluid Mechanics*, *44*, 123–142.

Nepf, & Vivoni (2000). Flow structure in depth-limited, vegetated flow. *Journal of Geophysical Research*, *105*(C12), 28,547–28,557.

Papke, A., & Battiato, I. (2013). A reduced complexity model for dynamic similarity in obstructed shear flows. *Geophysical Research Letters*, *40*, 3888–3892. https://doi.org/10.1002/grl.50759

Plew, D. R. (2010). Depth-averaged drag coefficient for modeling flow through suspended canopies. *Journal of Hydraulic Engineering*, *137*(2), 234–247.

Poggi, D., Katul, G., & Albertson, J. (2004). Momentum transfer and turbulent kinetic energy budgets within a dense model canopy. *Boundary-Layer Meteorology*, *111*(3), 589–614.

Poggi, D., Krug, C., & Katul, G. G. (2009). Hydraulic resistance of submerged rigid vegetation derived from first-order closure models. *Water Resources Research*, *45*, W10442. https://doi.org/10.1029/2008WR007373

Poggi, D., Porporato, A., Ridolfi, L., Albertson, J., & Katul, G. (2004). The effect of vegetation density on canopy sub-layer turbulence. *Boundary-Layer Meteorology*, *111*(3), 565–587.

Randall, C. W., Barnard, J. L., & Stensel, H. D. (1998). *Design and retrofit of wastewater treatment plants for biological nutrient removal*, vol. 5. Lancaster, PA: CRC Press.

Raupach, M., Finnigan, J., & Brunet, Y. (1996). Coherent eddies and turbulence in vegetation canopies: the mixing-layer analogy. *Boundary-Layer Meteorology*, *78*, 351–382.

Rubol, S., Battiato, I., & de Barros, F. P. (2016). Vertical dispersion in vegetated shear flows. *Water Resources Research*, *52*, 8066–8080. https://doi.org/10.1002/2016WR018907

Rubol, S., Ling, B., & Battiato, I. (2018). Universal scaling-law for flow resistance over canopies with complex morphology. *Scientific Reports*, *8*(1), 4430.

Sun, L., Liu, Y., & Jin, H. (2009). Nitrogen removal from polluted river by enhanced floating bed grown canna. *Ecological Engineering*, *35*(1), 135–140.

Teal, M. J., Ettema, R., & Walker, J. F. (1994). Estimation of mean flow velocity in ice-covered channels. *Journal of Hydraulic Engineering*, *120*(12), 1385–1400.

Wang, & Chen (2017). Contaminant transport in wetland flows with bulk degradation and bed absorption. *Journal of Hydrology*, *552*, 674–683.

Wang, H., & Huai, W. (2018). Analysis of environmental dispersion in a wetland flow under the effect of wind: Extended solution. *Journal of Hydrology*, *557*, 83–96.

Wells, G., Shi, Y., Laureni, M., Rosenthal, A., et al. (2017). Comparing the resistance, resilience, and stability of replicate moving bed biofilm and suspended growth combined nitritation–anammox reactors. *Environmental Science & Technology*, *51*(9), 5108–5117.

Yang, J. Q., Kerger, F., & Nepf, H. M. (2015). Estimation of the bed shear stress in vegetated and bare channels with smooth beds. *Water Resources Research*, *51*, 3647–3663. https://doi.org/10.1002/2014wr016042

Zeng, L., & Chen, G. (2011). Ecological degradation and hydraulic dispersion of contaminant in wetland. *Ecological Modelling*, *222*(2), 293–300.

Zhao, M., Huai, W., Han, J., Xie, Z., & Guo, J. (2012). Uniform laminar wetland flow through submerged and floating plants. *Journal of Hydraulic Research*, *50*(1), 52–59.